Full length article

Dislocation slip transmission through a coherent Σ3{111} copper twin boundary: Strain rate sensitivity, activation volume and strength distribution function

N.V. Malyar, B. Grabowski, G. Dehm, C. Kirchlechner[*]

Max-Planck-Institut für Eisenforschung GmbH, Max-Planck-Str. 1, 40237, Düsseldorf, Germany

A B S T R A C T

We present the first measurement of the strain rate sensitivity of the ideal dislocation slip transmission through a coherent Σ3{111} copper twin boundary. For this purpose we have deformed 129 geometrically identical samples at different strain rates. The micron-sized samples are either single crystalline (87 pillars) or contain one vertical Σ3{111} twin boundary (42 pillars). The strain rate sensitivity of the ideal slip transmission event is 0.015 ± 0.009. This value is considerably lower than the strain rate sensitivity observed for nano-twinned bulk materials, which is addressed to multiple simultaneously activated deformation processes present in the latter case. The activation volume of the ideal slip transmission points towards a cross-slip like transmission process of dislocations through the twin boundary. Furthermore, the high number of geometrically identical samples is used to discuss the ability to identify the strength distribution function of micropillars.

© 2018 Acta Materialia Inc. Published by Elsevier Ltd. This is an open access article under the CC BY-NC-ND license (http://creativecommons.org/licenses/by-nc-nd/4.0/).

1. Introduction

The impact of grain and twin boundaries (TBs) on the mechanical response of structural materials has widely been discussed during the last decades [1–4]. For instance, nanostructured face centered cubic materials containing multiple TBs possess unique properties like high strength and, simultaneously, high ductility [5]. All observed properties are likely caused by an interplay of lattice dislocations with TBs during dislocation motion, multiplication and annihilation. The quantitative contributions of individual processes are, however, not thoroughly understood [6].

In face centered cubic systems, like copper, {111}<110> dislocations can exhibit two transmission modes. In the "ideal" or "soft" mode, a lattice dislocation can transmit through the TB because its Burgers vector is conserved in both grains. In the "hard" mode the Burgers vector of the dislocation in the first grain (a lattice vector of the grain) is not a low-indexed lattice vector in the second grain, thus, slip is incompatible and, therefore, transmission is complicated. As a consequence, the latter case requires considerably higher transmission stresses as reported in detail in Refs. [7] and

[8]. Besides, dislocation-TB interactions can cause the loss of a nano-twinned microstructure often denoted as detwinning (e.g. in Ref. [9]) or the absorption of dislocations at the TB [7].

Within this work we focus on the ideal slip transmission mode of TBs, which was previously investigated computationally by atomistic modelling [7,10,11] as well as experimentally on TB containing micropillars [12–15]. Jin et al. [7] predict a slip transfer for copper as schematically shown in Fig. 1a. Lattice dislocations are split into their Shockley partials in the first grain and approach the boundary. At the TB the partials need to constrict to form a perfect dislocation having a common Burgers vector in both grains. After dislocation transmission, which according to Jin et al. requires shear stresses of 510 MPa in copper, the dislocation again splits into two partials. The aforementioned process is strongly reminiscent of cross-slip in a Friedel-Escaig manner [16–18], but was never observed experimentally. Also, the shear stress τ required to constrict two partial dislocations and enable cross-slip in copper was experimentally measured to be 24 ± 2 MPa, as reported by Caillard et al. [16]. This transmission stress is at least one order of magnitude smaller than the previously mentioned predictions from atomistic simulations.

To shed light on this discrepancy, *in situ* micro compression tests applying scanning electron microscopy (SEM) [12,19], transmission electron microscopy (TEM) [13] and synchrotron based x-ray Laue

* Corresponding author. Max-Planck-Institut für Eisenforschung GmbH, Max-Planck-Str. 1, D-40237, Düsseldorf, Germany.
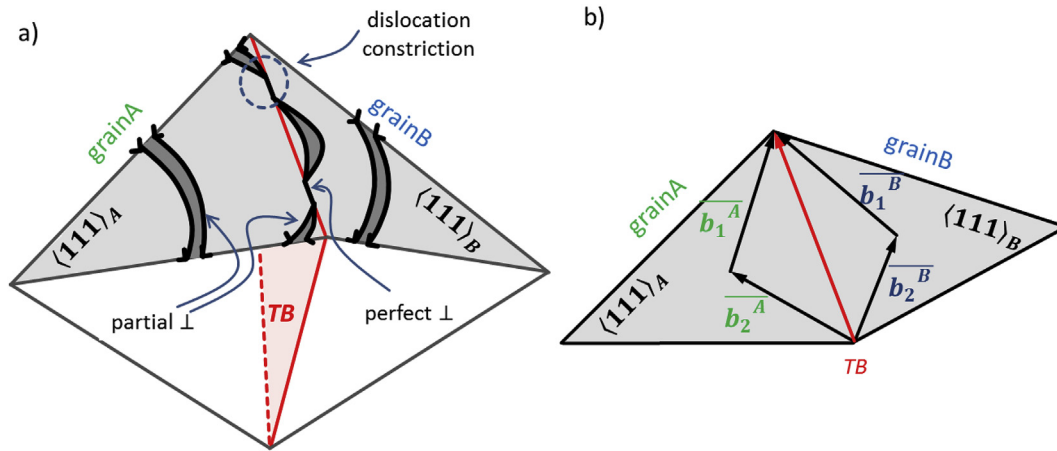*E-mail address:* kirchlechner@mpie.de (C. Kirchlechner).

Fig. 1. Ideal dislocation slip transfer strongly reminiscent of cross slip-like behavior (similar to the Friedel-Escaig mechanism) schematically shown on two Thompson tetrahedra: (a) dislocation lines and (b) 2D projection of the Burgers vectors. Only screw dislocations can transmit in the adjacent grain.

microdiffraction [14] experiments on micro pillars containing only one TB were performed recently. Common to all these experiments is the fact, that the TB containing pillars show similar stress-strain response as their single crystalline references, i.e. comparable yield stress and apparent strain hardening. The TEM experiments of Imrich et al. [13] revealed slip transmission without formation of a dislocation pile-up at engineering stresses significantly higher than 500 MPa. These high stresses are required for dislocation source activation within the submicron sized TEM samples. Any transmission stress lower than the observed stresses would not require a dislocation pile-up, hence, only an upper bound of the transmission stress can be specified from these *in situ* TEM experiments. In contrast, Malyar et al. used *in situ* μLaue diffraction to probe the dislocation transmission in several micrometer sized, TB containing bi-crystals. Measuring the local misorientation angle of the TB with the outstanding angular resolution of μLaue diffraction (~0.005°) they found (i) the absence of a dislocation pile-up at the boundary and (ii) simultaneously measured the global shear stress applied to the micro pillar. From their observations Malyar et al. concluded that ideal dislocation transmission can occur at shear stresses as low as 17 MPa [14].

Yet, these insights from *in situ* micro deformation of a coherent Σ3 TB contradict the picture drawn by nano-twinned bulk materials with superior strength and ductility solely caused by the presence of TBs [1]. Consequently, the key question is to find the fundamental origin of this tremendous discrepancy in flow stress. One remarkable difference between the deformation of small scale samples with respect to bulk nano-twinned systems is the local displacement rate, which might be orders of magnitude different in macro compared to the micro scale samples. Hence, a high strain rate sensitivity (SRS) of the dislocation TB interaction could explain the discrepancy of the observed nano-twinned bulk behavior with respect to the micron sized pillars. Lu et al. [2] were the first to point out the extreme SRS of up to 0.036 ± 0.009 in bulk nano-twinned copper by nano-indentation, which is considerably larger than the values observed for coarse grained ($m = 0.005-0.010$ [5,20,21]) and for single crystalline ($m = 0.01$ [22]) copper. However, due to the complex stress state beneath an indenter, nanoindentation causes the simultaneous activation of several different dislocation-TB interactions (e.g. ideal and hard slip transmission, detwinning, dislocation accumulation in the TB). While Lu's data [2] is representative for bulk nano-twinned materials, it cannot be used to judge on the SRS of one specific dislocation-TB interaction mechanism. Consequently, in this work

we aim for measuring the SRS of the ideal dislocation slip transmission through a coherent copper Σ3{111} copper TB by micro pillar compression.

2. Experimental details

Bulk bi-crystalline samples containing only one vertical coherent Σ3{111} TB were fabricated by the Bridgman technique from 99,88 at% purity copper. To minimize dislocation-dislocation interactions a crystallographic compression axis of <347> — being a single slip orientation — was selected. Thin slices of bi-crystalline sample were grinded, polished and electrochemically etched in phosphoric acid applying voltage of 15 V. The parameters where tuned to avoid any noticeable surface steps at the TB. Microsample preparation was done by focused ion beam (FIB) milling varying the current values from 16 nA down to 120 pA. The nominal sample size corresponds to $2.9 \pm 0.13\,\mu m^1$ and the aspect ratio of the pillars was kept in between $^1/_{2.3}...^1/_{3.8}$ to avoid buckling [23,24]. In total, we have successfully produced and tested 87 single crystalline pillars (denoted SX pillars) and 42 pillars containing a TB (denoted TB pillars). Compression tests were conducted using an ASMEC UNAT 2 indenter equipped with a flat punch tip of 5 μm in diameter and operated in displacement controlled mode. The strain rate was nominally varied from $1 \cdot 10^{-4}\,s^{-1}$ to $1 \cdot 10^{-1}\,s^{-1}$. The mean of top and bottom cross section diameters of each sample was taken as representative diameter to calculate the engineering stress values. To exclude the unwanted impact of extensive dislocation pile-ups and strain hardening, as well as assure slip transmission events we limit our discussion on engineering stress values extracted at engineering strains of 2%, further denoted as $\sigma_{2\%}$. Compression tests are followed with *post mortem* imaging, verifying the glide steps crystallography.

3. Results and interpretation

3.1. Strength of SX and TB pillars

The engineering stress versus strain data of the SX and the TB pillars appear on the first glance identical (Fig. 2a) showing

---

[1] All error bars are given as the standard error of the mean (*SE*) defined as statistical standard deviation (*s*) divided by the square root of the sample number (*N*): $SE = \frac{1}{\sqrt{N}}s$.

characteristic features well-known from the sample size effect era [25–27]. These features comprise serrated flow, a stochastic distribution of the flow stresses of nominally identical samples, and an increased strength with respect to bulk single crystalline copper. For further analysis we have plotted the cumulative probability function of the $\sigma_{2\%}$ stress of SX and TB containing pillars (Fig. 2b). Since the SX pillars of grain A and grain B have identical compression direction, comparable dislocation densities and — according to a "Kolmogorov-Smirnov goodness-of-fit" test [28] — statistically identical mechanical properties, they are summarized as "single crystals" and treated as one population. A smooth and almost symmetric distribution of the SX and TB pillars' $\sigma_{2\%}$ stress is observed. However, TB pillars deform at slightly higher stress values: The median of the TB is shifted to higher stress values with respect to the SX pillars — irrespective of the strain rate — between 11 and 16 MPa. The observed shift in normal stress translates to a difference in shear stress $\Delta\tau$ of 5–7 MPa (see Table 1). Besides, the two distributions largely overlap. From this viewpoint it is not surprising, that neither the representative curves shown in Fig. 2a, nor the former work of Imrich et al. [19] and Malyar et al. [14] took notice of the subtle differences of the SX and TB containing pillars. Recently, a comparable shift was reported by Liebig et al. for 110 oriented TB containing micropillars [15].

3.2. Distribution function of the yield stress in micropillars

Before discussing the SRS of the ideal dislocation slip transmission we want to focus on another key question in small scale
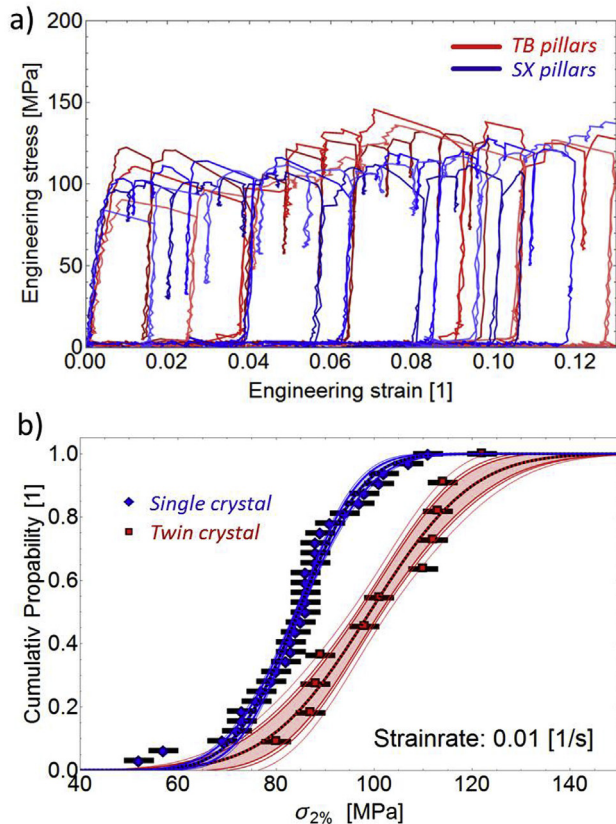

Fig. 2. (a) Engineering stress vs. strain diagram of 3 SX and 3 TB pillars. Neither the strength nor the apparent strain hardening of the SX and TB pillars allow for a discrimination of the two pillar sets. (b) The cumulative probability of the 2% engineering flow stress is plotted. The dashed lines show the best fit to a normal distribution. The 90, 95 and 99% confidence intervals of the fit are plotted by thin solid lines.

plasticity which possibly can be answered based on such a large dataset with nominally identical samples: What is the distribution function of the yield stress in micropillars? This is particularly interesting as it would enable an identification of the statistical dislocation source behavior e.g. obtained by discrete dislocation dynamics simulations [29] and, therefore, would allow for an in-depth understanding of the mechanisms limiting plasticity at the micron scale. For that purpose we have applied the Mathematica® "FindDistribution" method to find the distribution function best describing our dataset. Thereby, on the first glance $\sigma_{2\%}$ seems to be best described by a normal distribution with mean values as summarized in Table 1. This observation holds true for SX and TB pillars irrespective of the strain rate. The obtained cumulative probability curve including its 90%, 95% and 99% confidence intervals of the fit is plotted on top of the data in Fig. 2b, showing the exceptional match of the normal distribution. However, it is emphasized that several different distributions (e.g. a Chi-Squared, a Cauchy, a Log-Normal and a Weibull distribution) show reasonable agreement (see Fig. 3). Based on a "Kolmogorov-Smirnov goodness-of-fit" test all aforementioned distributions can explain the dataset with reasonable confidence and, also with bare eyes, it is impossible to judge on the underlying distribution function (see Fig. 3). If an identification of the underlying distribution function by *in situ* micromechanics is possible or not is discussed in chapter 4.3.

3.3. Strain rate sensitivity of SX and TB pillars

We have applied the aforementioned testing and analysis protocol with varying strain rate ($\dot{\varepsilon}$) ranging from $10^{-1}s^{-1}$ to $10^{-4}s^{-1}$, in order to measure the SRS of the ideal slip transmission process. In all cases the slip geometry did not change, i.e. at both sides of the TB the dove-tail shaped slip planes exhibit the same height (see Fig. 4) indicating that the intended ideal slip transfer took place. The number of formed slip steps varies from sample to sample, however, no systematic trend with strain rate can be identified. The corresponding stress-strain behavior of the SX pillars (Fig. 5a) and TB containing pillars (Fig. 5b) deformed at different strain rates follow the aforesaid behavior in terms of yield stress, yield stress distribution and apparent strain hardening.

To analyze the SRS, a logarithmic stress vs. logarithmic strain rate plot is applied as shown in Fig. 6, where the slope of the linear fit represents the SRS m calculated according to:

$$m = \frac{\partial \ln \sigma_{2\%}}{\partial \ln \dot{\varepsilon}} \tag{1}$$

The SRS of the SX pillars at 2% engineering strain is 0.007 ± 0.008. Thus, within the statistical errors, the measured SRS is similar to the previously found value for differently oriented SX pillars (0.01 ± 0.01) [30], and reasonably close to values obtained from coarse grained bulk copper which is typically ranging from 0.005 to 0.010 [5,20,21].

The SRS of the TB containing pillars is $m_{TB} = 0.015 \pm 0.009$ and will further be discussed in chapter 4.2.

4. Discussion

4.1. Why are TB pillars stronger than SX pillars?

The shift to higher stresses for the TB pillars can be caused by truncated dislocation source size in the TB pillars or by the barrier strength of the TB for ideal slip transmission. For penetrable high angle grain boundaries we recently showed that the grain size — defined as the maximum sphere which can be inscribed in each grain — dominates the initial deformation behavior for both, SX and

Table 1
Summary of the $\sigma_{2\%}$ stress distribution for SX and TB pillars at various strain rates: The parameters describe the best fit and standard error of a normal distribution. N equals the number of measured micro pillars.

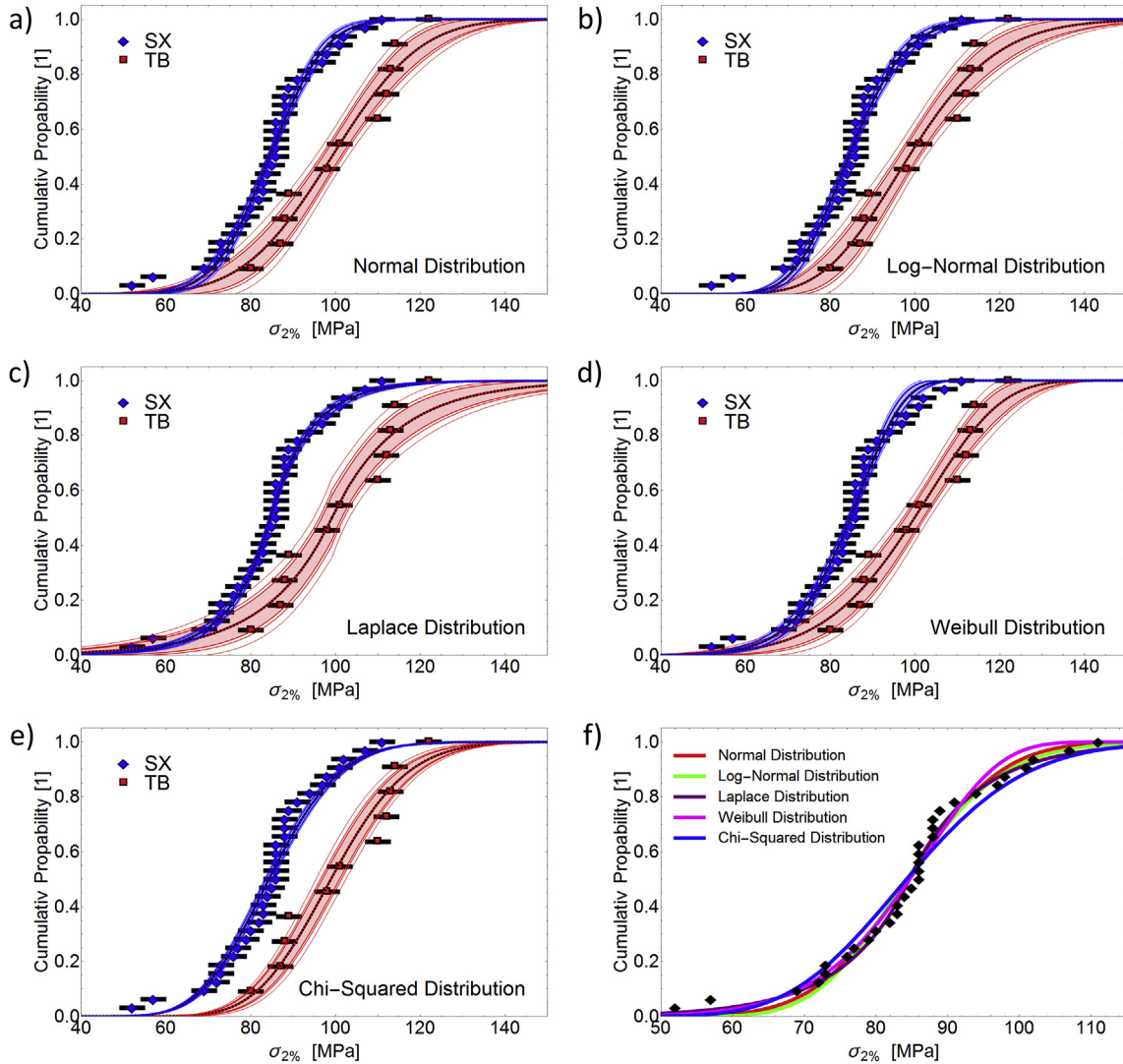| strain rate [1/s]		$\sigma_{2\%}$ SX [MPa]			$\sigma_{2\%}$ TB [MPa]			$\Delta\sigma_{2\%}$ [MPa]	$\Delta\tau_{2\%}$ [MPa]
nominal	regime	mean	st. dev.	N	mean	st. dev.	N		
10^{-4}	$5\ 10^{-5} - 5\ 10^{-4}$	$80{,}0 \pm 0{,}5$	$14{,}6 \pm 0{,}9$	22	$91{,}7 \pm 0{,}3$	$4{,}3 \pm 0{,}6$	10	$11{,}7 \pm 0{,}8$	$5{,}2 \pm 0{,}3$
10^{-3}	$5\ 10^{-4} - 5\ 10^{-3}$	$88{,}3 \pm 0{,}3$	$11{,}8 \pm 0{,}5$	23	$100{,}6 \pm 1{,}3$	$14{,}2 \pm 2{,}0$	14	$12{,}2 \pm 1{,}5$	$5{,}4 \pm 0{,}7$
10^{-2}	$5\ 10^{-3} - 5\ 10^{-2}$	$84{,}5 \pm 0{,}3$	$10{,}4 \pm 0{,}5$	32	$99{,}1 \pm 1{,}1$	$16{,}4 \pm 1{,}7$	11	$14{,}7 \pm 1{,}4$	$6{,}5 \pm 0{,}6$
10^{-1}	$5\ 10^{-2} - 5\ 10^{-1}$	$91{,}1 \pm 1{,}5$	$18{,}6 \pm 2{,}7$	10	$107{,}2 \pm 2{,}3$	$12{,}9 \pm 3{,}6$	7	$16{,}1 \pm 3{,}8$	$7{,}1 \pm 1{,}7$

Fig. 3. Comparison the cumulative probability of SX and TB pillars and various distribution functions: (a) Normal distribution; (b) Log-Normal distribution; (c) Laplace distribution; (d) Weibull distribution and (e) Chi-Squared distribution. Furthermore, the best fit to the SX data is shown in (f) for comparison.

bi-crystalline pillars containing a penetrable grain boundary [31]. This behavior was explained by the maximum dislocation source size being able to operate. In case of an SX pillar the maximum dislocation source size scales with the pillar diameter (Fig. 7, left). In case of a general high angle grain boundary containing pillar (Fig. 7 right), the maximum dislocation source size scales with the grain size (i.e. scales with half the pillar diameter). The decreased dislocation source size requires higher source activation stresses in the latter case, which results in a strength increase of bi-crystalline pillars with respect to their single crystalline counter bodies. The stress difference caused by this dislocation truncation, $\Delta\sigma_{\text{truncation}}$, can be quantified by assuming a unique size scaling of copper following the empirical size scaling law $\sigma(d) = \sigma_0 + \frac{k}{d^m}$, with $\sigma_0 = 15$ MPa, $m = 0.68 \pm 0.07$ and $k = 171 \pm 10$ MPa μm^m (describing the data in Ref. [31]). When the dislocation source size is strictly truncated by the TB, the expected strength increase of the TB with respect to the SX samples can be calculated, $\Delta\sigma_{\text{truncation}} = \sigma_{\text{TB}} - \sigma_{\text{SX}} = \sigma(1.5\ \mu m) - \sigma(3.0\ \mu m) = 49 \pm 22$ MPa ($\Delta\tau_{\text{truncation}} = 21.4 \pm 10$ MPa). The predicted $\Delta\tau_{\text{truncation}}$ is considerably larger than the observed shift $\Delta\tau_{2\%} \approx 7$ MPa as presented in Fig. 2b
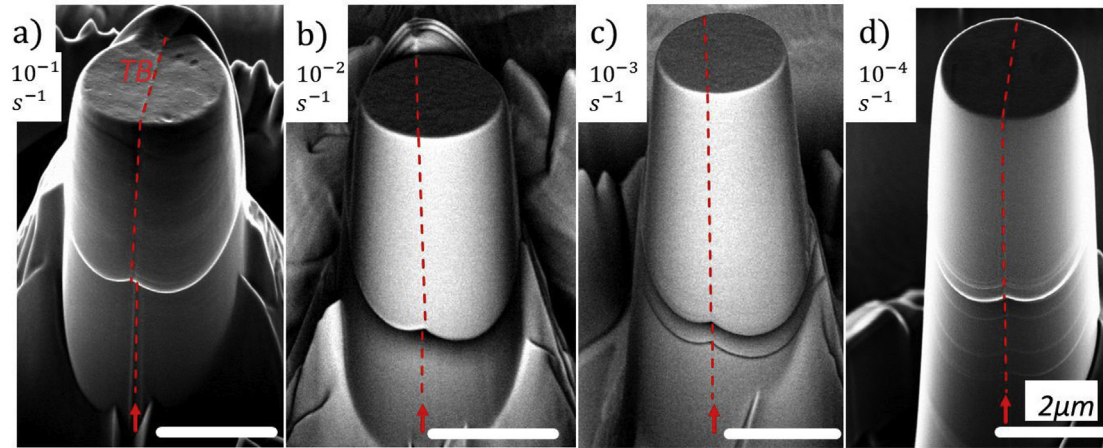
Fig. 4. Post mortem secondary electron SEM images of TB pillars compressed to a strain of approximately 9–12% at a strain rate of (a) $10^{-1}s^{-1}$, (b) $10^{-2}s^{-1}$, (c) $10^{-3}s^{-1}$, and (d) $10^{-4}s^{-1}$. The position of TB is highlighted in red. (For interpretation of the references to colour in this figure legend, the reader is referred to the Web version of this article.)
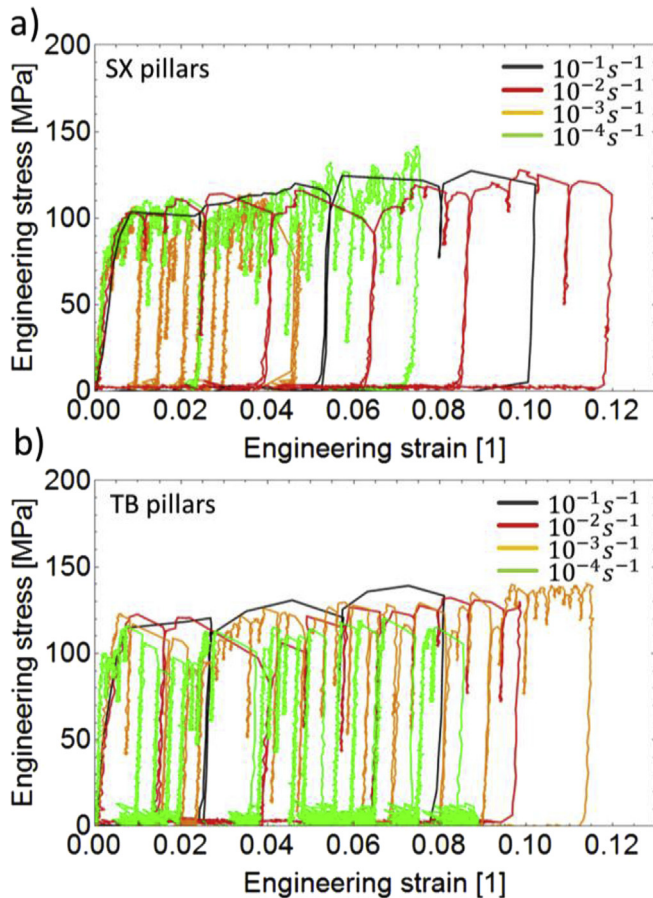

Fig. 5. Engineering stress-strain diagrams of (a) single crystalline (SX) pillars and (b) twin boundary containing (TB) pillars deformed at different strain rates. A weak SRS and absence of apparent hardening is visible.

Fig. 6. Strain rate sensitivity plot for single crystalline (SX) and twin boundary containing (TB) micropillars. Besides the best fit (dashed line) also 90%, 95% and 99% confidence intervals of the fit are given.

and Table 1. Consequently, a strict dislocation source size truncation by the grain size (Fig. 7, right) does not take place in the studied TB pillars. Instead, in the absence of dislocation pile-ups [14], dislocation sources have to expand through the TB during dislocation multiplication (Fig. 7, center).

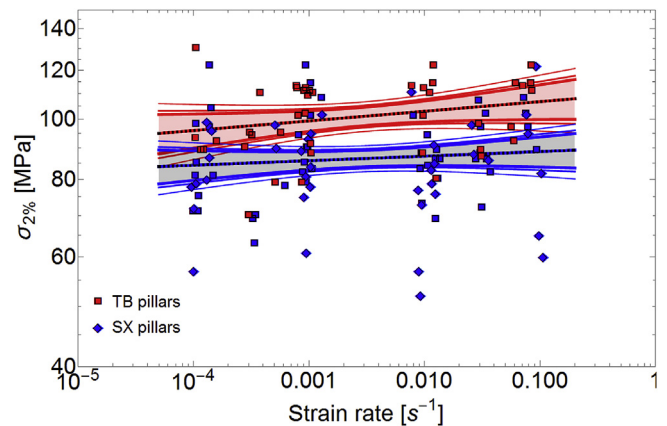The dislocation source expanding through the TB looks differently than a dislocation source in a SX pillar (see Fig. 7): While dislocation sources in SX pillars exhibit a continuous curvature, their counter bodies in TB pillars have to constrict at the TB to form a perfect screw dislocation. This constriction is required for dislocation slip transmission in a cross-slip-like manner. Hence, in the TB pillars the dislocation source will exhibit a double-hump shape (see Fig. 7, center). Due to the formed double-hump, dislocation sources in the TB pillars experience an increased curvature with respect to the continuous dislocation source in the SX case. As a consequence, TB containing pillars exhibit a marginally higher shear stress. The experimental proof and quantification of the double-hump in micron sized samples is experimentally challenging and was not focus of this work. Nevertheless, the increase of $\Delta\tau$ with strain rate (see Table 1) qualitatively supports the double-hump model.

Our current work shows that the contributions of dislocation multiplication and transmission to the overall strength of a TB pillar can certainly not be separated easily: The lowest measured transmission shear stress reported by Malyar et al. ($\tau_{\text{transmission}} \geq 17$ MPa) [14] and the one estimated from a dislocation cross-slip-like mechanism in a Friedel-Escaig manner as described by Caillard et al. ($\tau = 24 \pm 2$ MPa) [16] are considerably larger than the shift in shear stress $\Delta\tau_{2\%} \approx 7$ MPa observed here. Hence, in our case, the sum of the SX strength and the transmission
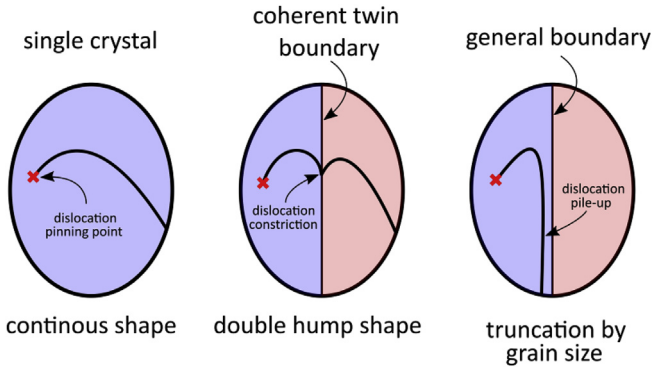
Fig. 7. Schematic showing a dislocation source operating in a single crystal, a bi-crystalline pillar containing a coherent TB and a bi-crystal with a general grain boundary. In the TB containing pillar the dislocation constriction required for slip transfer is causing a double-hump. For clarity only a full dislocation instead of the partials and the stacking fault are shown.

stress does not predict the strength of the TB pillar ($\tau_{TB} \neq \tau_{SX} + \tau_{transmission}$). In view of this observation it is highly questionable if a simple sum of individual strengthening mechanisms can ever be used as a predictor for the strength of bi-crystalline pillars.

4.2. Strain rate sensitivity of slip transmission and activation volume

The SRS $m_{TB} = 0.015 \pm 0.009$ is considerably lower than 0.036 ± 0.009 found by L. Lu and co-workers via nanoindentation on nano-twinned materials with a twin spacing of 20 nm. Also the mean SRS of 0.025 ± 0.009 of Lu's "lower twin density" with a spacing of 90 nm is − even though with an overlap of the error bars − higher than the value observed in our study. As stated in the introduction, the simultaneous activation of ideal and hard dislocation transmission in the ultrafine grained polycrystals, the presence of dislocation absorption and likely detwinning, as well as the heterogeneous stress state during nanoindentation offer ample mechanism-based explanations for the observed differences. Lu's nano-twinned systems exhibit a SRS similar to our previous penetrable high angle grain boundary ($m = 0.04 \pm 0.02$) [30], which requires non-conservative slip of dislocations in the grain boundary. Another explanation based on the SRS of cross-slip in nano-twinned systems is offered by Asaro and Kulkarni [32]. They propose an SRS of the dislocation cross-slip-like transmission event with increasing SRS with smaller twin spacing. Nevertheless, we were not able to verify this theory based on our micron sized micropillar experiments which was conducted on only one pillar size.

The comparable SRS of the SX and TB pillars also indicate, that the tremendous difference of the transmission stresses obtained from atomistic simulations [7,10] and from experiments [14] can − despite the tremendous differences in strain rate in simulations and experiments − likely not be explained by strain-rate effects. It can be speculated that the use of periodic boundary conditions complicates the dislocation transmission by zipping through the boundary − similar as shown by the double-hump in Fig. 7.

In our case the obtained SRS is − in light of the observed ideal slip transmission − representative for the SRS of the ideal slip transmission process. As initially stated, such an ideal slip transmission can be envisioned similarly to a cross-slip-like process in a Friedel-Escaig manner. However, this process was experimentally never observed. To quantitatively compare our results with literature we will use the activation volume v^* defined as

$$v^* = \frac{\sqrt{3}kT}{m\,\sigma}, \tag{2}$$

with the Boltzmann constant k and the absolute testing temperature T. The ideal slip transmission through the TB exhibits an activation volume of $v^*_{TB} = 440 \pm 260\,b^3$, with b representing the Burgers vector of copper. Despite the large experimental error on the activation volume, our results are in accordance with the data obtained from Bonneville et al. [33,34] for cross-slip in pure copper ($280 \pm 65\,b^3$). The comparable activation volume for dislocation cross-slip and ideal slip transmission point towards a similar nature of the dislocation slip transmission event and therefore support our view on a cross-slip-like transmission.

In contrast, the activation volume measured in SX pillars is $v^*_{SX} = 700\,b^3$ with a lower bound estimate of $325\,b^3$. Since the lower bound value for the SRS of SX pillars is close to zero, a meaningful upper bound for the SX activation volume cannot be provided here. Nevertheless, despite the large error bars, the activation volumes obtained in the SX and for cross-slip [33,34] overlap only marginally. This indicates that cross-slip is likely − as expected − not the rate dominating process in SX micropillars.

4.3. Can we discriminate the SRS of SX and TB pillars?

To clearly discriminate the SRS of SX and TB containing pillars the sum of both standard errors (SE) needs to be smaller than the difference of the SRS:

$$SE_{SX} + SE_{TB} \leq \Delta m, \tag{3}$$

where $\Delta m = m_{SX} - m_{TB} = 0.008$. We further assume that the standard deviations s of the SX and TB containing pillars are − as shown in Table 1 − comparable and remain unchanged at high sample numbers. Due the relation $s = SE \cdot \sqrt{N}$ one can estimate the standard error SE_2 at a sample number N_2 from the SE_1 obtained at the lower sample number N_1 by:

$$SE_2 = SE_1 \sqrt{N_1/N_2} \tag{4}$$

Furthermore, we assume that further testing follows the same protocol as the previous tests, i.e. the number of tested TB pillars is half the number of tested SX pillars, Eq. (3) can then be rewritten as:

$$\sqrt{N_1/N_2}\,(SE_{SX,1} + SE_{TB,1}) \leq \Delta m \tag{5}$$

Solving Eq. (5) for the number of TB containing pillars using $N_1 = 42$, the standard error and Δm as listed in Table 1 leads to $N_2 \geq 189$ TB pillars. Therefore, a total number of roughly 600 samples (~400 SX and ~200 TB containing pillars) are at least required to probe the modest differences in the SRS of SX and TB pillars. As this high number of geometrically identical pillars is currently out of reach for micro pillar compression, a statistically sound answer on the differences of SX and TB containing pillars cannot be given here. However, the data obtained from 128 samples suggests minor differences in the SRS of single crystals and coherent $\Sigma3\{111\}$ TB containing copper pillars oriented for ideal slip transmission.

4.4. How many samples are required to identify the strength-distribution function?

Finally, let us discuss the number of samples required to identify the strength distribution function of micropillars: Based on the sample number tested within this study at a given strain rate we are

not able to conclusively identify the distribution (see Fig. 3). But how long would we have to continue testing to get conclusive results? Clearly, the sample number required to identify the distribution function (N_{req}) strongly depends on the underlying distribution function and its parameters, hence, a general answer cannot be provided here. Nevertheless, for our samples we estimate N_{req} using the subsequent Monte-Carlo approach.

First, we assume that our SX pillar strength $\sigma_{2\%}$ at a strain rate of 10^{-3} s^{-1} is Weibull distributed,

$$p_W(\sigma_{2\%}) = \sigma_{2\%}{}^{\alpha-1} \, e^{-(\sigma_{2\%}/\beta)^{\alpha}} \qquad (6)$$

with the parameters $\alpha = 9.4$ and $\beta = 88$ MPa following the experimental findings of $\alpha_{exp} = 9.41 \pm 0.53$ and $\beta_{exp} = 88.05 \pm 0.31$ MPa. We randomly generated Weibull distributed pillar sets with N samples (N is ranging from 5 to 1000). Subsequently, we applied a "Kolmogorov-Smirnoff goodness-of-fit" test for several distribution functions (e.g. Normal, Log-Normal, Laplace distribution). A Kolmogorov-Smirnoff probability (p_{KS}) below the significance level of 0.05 is interpreted as a bad fit, i.e. the applied distribution function cannot describe the random (Weibull distributed) data. If $p_{KS} > 0.05$ the test is inconclusive and the applied distribution function could still be used to describe the underlying dataset.

The results of this Monte-Carlo simulation are presented in Fig. 8a, where the sample number is plotted versus the mean p_{KS} of 1000 random data sets, $\overline{p_{KS}}$. It can be seen that the 0.05 confidence level of the Normal and Log-Normal distribution is crossed at roughly $N_{req} = 300$ samples. Hence, if $\sigma_{2\%}$ is Weibull distributed with the aforementioned parameters, on average we would need 300 geometrically identical samples to exclude a Normal and a Log-Normal distribution. For a Laplace distribution we would require more than $N_{req} = 500$ samples (see Fig. 8a).

An alternative view on the required sample number N_{req} is shown in Fig. 8b. Here, the probability of having a conclusive result $p_{conclusive}$ is the ratio of the number of conclusive datasets (with $p_{KS} < 0.05$) to all randomly generated datasets. While for small datasets ($N < 100$) the Laplace and Log-Normal distributions can never be excluded, only huge datasets ($N > 500$) have a high probability to uniquely identify the strength distribution. Hence, within standard micromechanical testing capacities an identification of the underlying distribution function is challenging and should be done by alternative methods, e.g. pop-in statistics using nanoindentation [35].

5. Summary and conclusion

In summary, the strain rate sensitivity (SRS) of single crystalline and coherent Σ3{111} twin boundary containing copper pillars was measured using *in situ* micro compression tests. From the 128 experiments the following conclusions can be drawn:

- The flow stress of twin boundary containing pillars is shifted by $\Delta\tau_{2\%} = 5 \dots 7$ MPa to higher shear stresses with respect to the single crystalline pillars. The shift is lower than the expectations from dislocation source size truncation in a bi-crystalline micropillar and lower than the experimentally observed transmission stress through coherent Σ3{111} boundaries [14]. We propose a double-hump dislocation shape required in twin boundary containing pillars resulting a slightly higher $\Delta\tau_{2\%}$.
- The SRS of the ideal slip transmission process ($m_{TB} = 0.015 \pm 0.009$) is considerably lower than the one in nano-twinned copper reported by Lu et al. [2] ($m = 0.036 \pm 0.009$) and lower than the one observed for dislocation slip transmission based on non-conservative dislocation
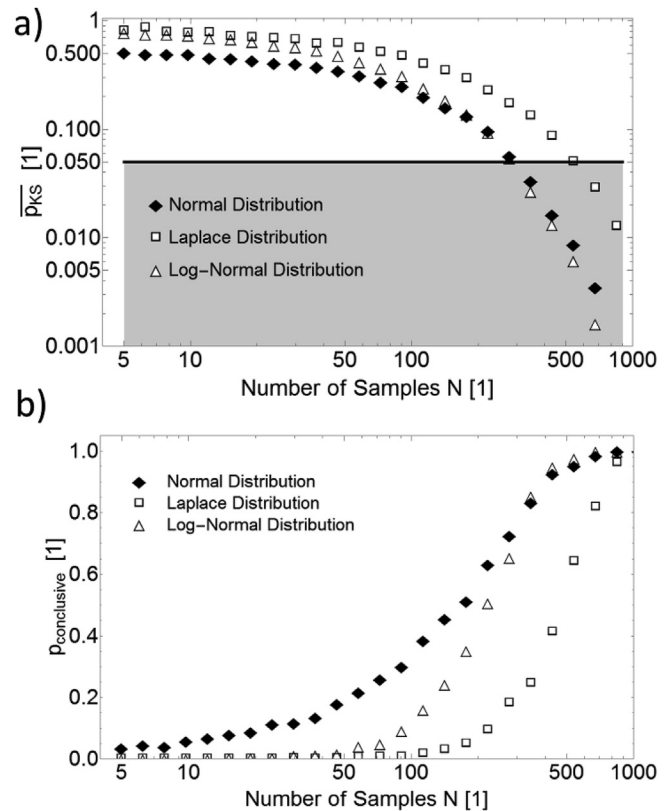

Fig. 8. a) "Kolmogorov-Smirnov goodness-of-fit" probability $\overline{p_{KS}}$ of a distribution describing a randomly generated Weibull distribution. The used significance interval ($p_{KS} = 0.05$, gray area) requires 300 to 500 samples to correctly identify the underlying distribution. b) Probability to correctly identify the distribution function of a Weibull distributed pillar population from other distributions (see text for details).

motion through penetrable high angle grain boundaries ($m = 0.04 \pm 0.02$) [30].

- The low SRS indicates that strain rate effects can − despite the tremendous differences in strain rate − not explain the quantitative differences in ideal dislocation transmission shear stresses obtained from atomistic simulations and experiments.
- The activation volume of the twin boundary containing crystals ($v^*_{TB} = 440 \pm 260 \, b^3$) is matching the activation volume for cross-slip (~280 b^3) well, strongly supporting our view on ideal slip transmission in a cross-slip-like manner.
- The SRS of single and twin boundary containing pillars is − within the error bars − indistinguishable ($m_{SX} = 0.007 \pm 0.008$ and $m_{TB} = 0.015 \pm 0.009$). Whether or not the SRS of the single crystalline and twin containing pillars are different would require a total number of around 600 micro compression samples (tested at different strain rates).
- To identify the strength distribution function of micropillars considerably more samples are required. For the presented case, at least 300 to 500 geometrically identical samples tested at the same strain rate are required to discriminate a Weibull distribution from a Normal, Log-Normal or Cauchy distribution.

References

[1] L. Lu, X. Chen, X. Huang, K. Lu, Revealing the maximum strength in nano-twinned copper, Science 323 (5914) (2009) 607—610.

[2] L. Lu, R. Schwaiger, Z.W. Shan, M. Dao, K. Lu, S. Suresh, Nano-sized twins induce high rate sensitivity of flow stress in pure copper, Acta Mater. 53 (7) (2005) 2169—2179.

[3] K. Lu, Stabilizing nanostructures in metals using grain and twin boundary architectures, Nature Reviews Materials 1 (2016).

[4] D. Jang, X. Li, H. Gao, J.R. Greer, Deformation mechanisms in nanotwinned metal nanopillars, Nat. Nanotechnol. 7 (9) (2012) 594—601.

[5] M. Dao, L. Lu, Y.F. Shen, S. Suresh, Strength, strain-rate sensitivity and ductility of copper with nanoscale twins, Acta Mater. 54 (20) (2006) 5421—5432.

[6] T. Zhu, H. Gao, Plastic deformation mechanism in nanotwinned metals: an insight from molecular dynamics and mechanistic modeling, Scripta Mater. 66 (11) (2012) 843—848.

[7] Z.H. Jin, P. Gumbsch, E. Ma, K. Albe, K. Lu, H. Hahn, H. Gleiter, The interaction mechanism of screw dislocations with coherent twin boundaries in different face-centred cubic metals, Scripta Mater. 54 (6) (2006) 1163—1168.

[8] Z.H. Jin, P. Gumbsch, K. Albe, E. Ma, K. Lu, H. Gleiter, H. Hahn, Interactions between non-screw lattice dislocations and coherent twin boundaries in face-centered cubic metals, Acta Mater. 56 (5) (2008) 1126—1135.

[9] J. Wang, N. Li, O. Anderoglu, X. Zhang, A. Misra, J.Y. Huang, J.P. Hirth, Det-winning mechanisms for growth twins in face-centered cubic metals, Acta Mater. 58 (6) (2010) 2262—2270.

[10] M. Chassagne, M. Legros, D. Rodney, Atomic-scale simulation of screw dislocation/coherent twin boundary interaction in Al, Au, Cu and Ni, Acta Mater. 59 (4) (2011) 1456—1463.

[11] J.B. Jeon, G. Dehm, Formation of dislocation networks in a coherent Cu Σ3(1 1 1) twin boundary, Scripta Mater. 102 (2015) 71—74.

[12] P.J. Imrich, C. Kirchlechner, G. Dehm, Influence of inclined twin boundaries on the deformation behavior of Cu micropillars, Mater. Sci. Eng. 642 (0) (2015) 65—70.

[13] P.J. Imrich, C. Kirchlechner, D. Kiener, G. Dehm, Internal and external stresses: in situ TEM compression of Cu bicrystals containing a twin boundary, Scripta Mater. 100 (0) (2015) 94—97.

[14] N.V. Malyar, J.S. Micha, G. Dehm, C. Kirchlechner, Dislocation-twin boundary interaction in small scale Cu bi-crystals loaded in different crystallographic directions, Acta Mater. 129 (2017) 91—97.

[15] J.P. Liebig, S. Krauß, M. Göken, B. Merle, Influence of stacking fault energy and dislocation character on slip transfer at coherent twin boundaries studied by micropillar compression, Acta Mater. 154 (2018) 261—272.

[16] D. Caillard, J.L. Martin, Some aspects of cross-slip mechanisms in metals and alloys, J. Phys. 50 (18) (1989).

[17] J. Friedel, Dislocations, Pergamn Press, 1964.

[18] B. Escaig, Université d'Orsay, Thesis, 1968.

[19] P.J. Imrich, C. Kirchlechner, C. Motz, G. Dehm, Differences in deformation behavior of bicrystalline Cu micropillars containing a twin boundary or a large-angle grain boundary, Acta Mater. 73 (0) (2014) 240—250.

[20] R.P. Carreker Jr., W.R. Hibbard Jr., Tensile deformation of high-purity copper as a function of temperature, strain rate, and grain size, Acta Metall. 1 (6) (1953), 654-"655,657-663".

[21] R.J. Asaro, S. Suresh, Mechanistic models for the activation volume and rate sensitivity in metals with nanocrystalline grains and nano-scale twins, Acta Mater. 53 (12) (2005) 3369—3382.

[22] J.Y. Zhang, X. Liang, P. Zhang, K. Wu, G. Liu, J. Sun, Emergence of external size effects in the bulk-scale polycrystal to small-scale single-crystal transition: a maximum in the strength and strain-rate sensitivity of multicrystalline Cu micropillars, Acta Mater. 66 (2014) 302—316.

[23] H. Zhang, B.E. Schuster, Q. Wei, K.T. Ramesh, The design of accurate micro-compression experiments, Scripta Mater. 54 (2) (2006) 181—186.

[24] C. Kirchlechner, F. Toth, F.G. Rammerstorfer, F.D. Fischer, G. Dehm, Pre- and post-buckling behavior of bi-crystalline micropillars: origin and consequences, Acta Mater. 124 (2017) 195—203.

[25] J.R. Greer, J.T.M. De Hosson, Plasticity in small-sized metallic systems: intrinsic versus extrinsic size effect, Prog. Mater. Sci. 56 (6) (2011) 654—724.

[26] O. Kraft, P.A. Gruber, R. Mönig, D. Weygand, Plasticity in confined dimensions, Annu. Rev. Mater. Res. 40 (2010) 293—317.

[27] M.D. Uchic, P.A. Shade, D.M. Dimiduk, Plasticity of micrometer-scale single crystals in compression, Annu. Rev. Mater. Res. 39 (2009) 361—386.

[28] W. Research, Mathematica, 2016.

[29] J.A. El-Awady, Unravelling the physics of size-dependent dislocation-mediated plasticity, Nat. Commun. 6 (2015).

[30] N.V. Malyar, G. Dehm, C. Kirchlechner, Strain rate dependence of the slip transfer through a penetrable high angle grain boundary in copper, Scripta Mater. 138 (2017) 88—91.

[31] N.V. Malyar, J.S. Micha, G. Dehm, C. Kirchlechner, Size effect in bi-crystalline micropillars with a penetrable high angle grain boundary, Acta Mater. 129 (2017) 312—320.

[32] R.J. Asaro, Y. Kulkarni, Are rate sensitivity and strength effected by cross-slip in nano-twinned fcc metals, Scripta Mater. 58 (5) (2008) 389—392.

[33] J. Bonneville, B. Escaig, Cross-slipping process and the stress-orientation dependence in pure copper, Acta Metall. 27 (9) (1979) 1477—1486.

[34] J. Bonneville, B. Escaig, J.L. Martin, A study of cross-slip activation parameters in pure copper, Acta Metall. 36 (8) (1988) 1989—2002.

[35] J.R. Morris, H. Bei, G.M. Pharr, E.P. George, Size effects and stochastic behavior of nanoindentation pop in, Phys. Rev. Lett. 106 (16) (2011) 165502.